European Journal of Medicinal Chemistry 136 (2017) 104–113

Contents lists available at ScienceDirect

European Journal of Medicinal Chemistry

journal homepage: http://www.elsevier.com/locate/ejmech

Research paper

Synthesis and preclinical evaluation of [^{11}C]MA-PB-1 for *in vivo* imaging of brain monoacylglycerol lipase (MAGL)

Muneer Ahamed [a, 1], Bala Attili [a, 1], Daisy van Veghel [a], Maarten Ooms [a], Philippe Berben [a], Sofie Celen [a], Michel Koole [b], Lieven Declercq [a], Juha R. Savinainen [c], Jarmo T. Laitinen [c], Alfons Verbruggen [a], Guy Bormans Prof. [a, *]

[a] *Laboratory for Radiopharmaceutical Research, Department of Pharmaceutical and Pharmacological Sciences, Campus Gasthuisberg O&N2, Herestraat 49 Box 821, BE-3000 Leuven, Belgium*
[b] *Department of Nuclear Medicine & Molecular Imaging, UZ Herestraat 49, 3000 Leuven, Belgium*
[c] *Institute of Biomedicine, Faculty of Health Sciences, The University of Eastern Finland, Finland*

ARTICLE INFO

Article history:
Received 8 February 2017
Received in revised form
21 April 2017
Accepted 24 April 2017
Available online 25 April 2017

Keywords:
MAGL
[^{11}C]MA-PB-1
MJN110
Biodistribution
PET imaging

ABSTRACT

MAGL is a potential therapeutic target for oncological and psychiatric diseases. Our objective was to develop a PET tracer for *in vivo* quantification of MAGL. We report [^{11}C]MA-PB-1 as an irreversible MAGL inhibitor PET tracer. The in vitro inhibitory activity, *ex vivo* distribution, brain kinetics and specificity of [^{11}C]MA-PB-1 binding were studied. Ex vivo biodistribution and microPET showed good brain uptake which could be blocked by pretreatment with both MA-PB-1 and a structurally non-related MAGL inhibitor MJN110. These initial results suggest that [^{11}C]MA-PB-1 is a suitable tracer for *in vivo* imaging of MAGL.

1. Introduction

The endocannabinoid system consists of cannabinoid receptors, endogenous ligands and other proteins for their synthesis, degradation and transport [1,2]. In the central nervous system, the endocannabinoid system plays an important role in the regulation of several physiological functions such as cognition, pain, movement and memory [3,4]. Two of the most important and widely studied endogenous lipid transmitters are *N*-arachidonoyl ethanolamine or anandamide (AEA) and 2-arachidonoylglycerol (2-AG) [5]. These two endocannabinoids are synthesized on demand in response to neuronal activity. The signal is then rapidly terminated due to the breakdown of the endocannabinoids by the enzymatic activity of two serine hydrolases: fatty acid amide hydrolase (FAAH) and monoacylglycerol lipase (MAGL), respectively [6].

MAGL is a 33-kDa cytosolic serine hydrolase enzyme that preferentially cleaves monoacylglycerols into fatty acids and glycerol and plays a crucial role in coordinating multiple lipid signalling pathways. In the brain, MAGL was found to be co-localized with CB1 receptors in axon terminals where it is responsible for approximately 85% of 2-AG hydrolysis [7,8]. Therefore, MAGL is an

Abbreviations: AA, arachidonic acid; AEA, N-arachidonoyl ethanolamine; 2-AG, 2-arachidonoyl glycerol; BBB, blood brain barrier; Bmax, enzyme expression; BBr_3, boron tribromide; CB1, cannabinoid 1 receptors; $CDCl_3$, deuterated chloroform; CH_3CN, acetonitrile; clog D, calculated distribution coefficient; cPSA, calculated polar surface area; Cs_2CO_3, cesium carbonate; DCM, dichloromethane; DIPEA, diisopropylethylamine; DMF, dimethylformamide; DMSO, dimethylsulfoxide; EtOAc, ethyl acetate; EtOH, ethanol; ESI, electron spray ionization; FAAH, fatty acid amide hydrolase; GBq/mmol, Gigabecquerel per micromole; hMAGL, human monoacylglycerol lipase; HRMS, high resolution mass spectrometry; IC_{50}, minimum inhibitory concentration (50% enzyme inhibition); K_D, dissociation constant; K_2EDTA, ethylenediaminetetraacetic acid dipotassium salt; LPA, lysophosphatidic acid; MAGL, monoacylglycerol lipase; MBq, megabecquerel; $MgSO_4$, magnesium sulfate; $NaBH(OAc)_3$, sodium triacetoxyborohydride; $NaHCO_3$, sodium bicarbonate; NaOAc, sodium acetate; NMR, nuclear magnetic resonance spectroscopy; NMRI, naval medical research institute; NaI(Tl), thallium-doped sodium iodide; PET, positron emission tomography; PGE_2, prostaglandin E_2; p.i., post injection; RP-HPLC, reverse phase-high performance liquid chromatography; SUV, standardized uptake value; TAC, time activity curve; TFA, trifluoroacetic acid; TMS, tetramethylsilane; UHPLC, ultra-high performance liquid chromatography; UHR-TOF, ultra-high resolution time of flight; VOI, volume of interest; %ID, percentage injected dose; [^{18}F]FDG, 2-[^{18}F]fluoro-2-deoxy-D-glucose; 3D-MAP, 3D maximum a posteriori iterative reconstruction.

* Corresponding author. O&N2, Herestraat 49, box 821, BE-3000 Leuven, Belgium.
E-mail address: guy.bormans@kuleuven.be (G. Bormans).

[1] These authors contributed equally.

http://dx.doi.org/10.1016/j.ejmech.2017.04.066
0223-5234/

important terminating factor of the endocannabinoid signalling activity. Additionally, MAGL also plays an important role in the release of arachidonic acid (AA) and other free fatty acids like prostaglandin E2 (PGE2) and lysophosphatidic acid (LPA). It is well established that AA is metabolized to pro-inflammatory prostaglandins and the free fatty acids generate pro-tumorigenic signalling lipids [9,10].

Because of its important role in several lipid signalling pathways, MAGL is known to be involved in many pathological conditions, such as inflammation, cancer, neurodegenerative disorders and several psychological disorders such as anxiety and depression [10]. Blockage of MAGL leads to increased 2-AG levels and enhanced endocannabinoid signalling [11]. Additionally, blockage of MAGL also lowers AA levels, which in turn leads to decreased production of pro-inflammatory prostaglandins. Therefore, MAGL inhibition could play an important role in several diseases. Indeed, previous studies have shown that MAGL blockade has several beneficial outcomes in inflammation, pain, anxiety, neurodegeneration and cancer [10,12–15]. In the recent past, a number of selective and potent MAGL inhibitors have been developed to modulate MAGL activity [16–20]. Cravatt et al. identified some interesting carbamate containing small molecule inhibitors of MAGL, particularly JW-642 was reported to have an IC_{50} value of 3.7 nM for *h*MAGL [16].

Non-invasive imaging of MAGL using positron emission tomography (PET) can assist in the translational evaluation of promising drug candidates targeting MAGL. Furthermore, PET imaging of MAGL also allows quantifying MAGL expression *in vivo* thus allowing to identifying modulation of MAGL in relevant pathologies. Therefore, the development of a suitable PET radioligand to visualize MAGL is important.

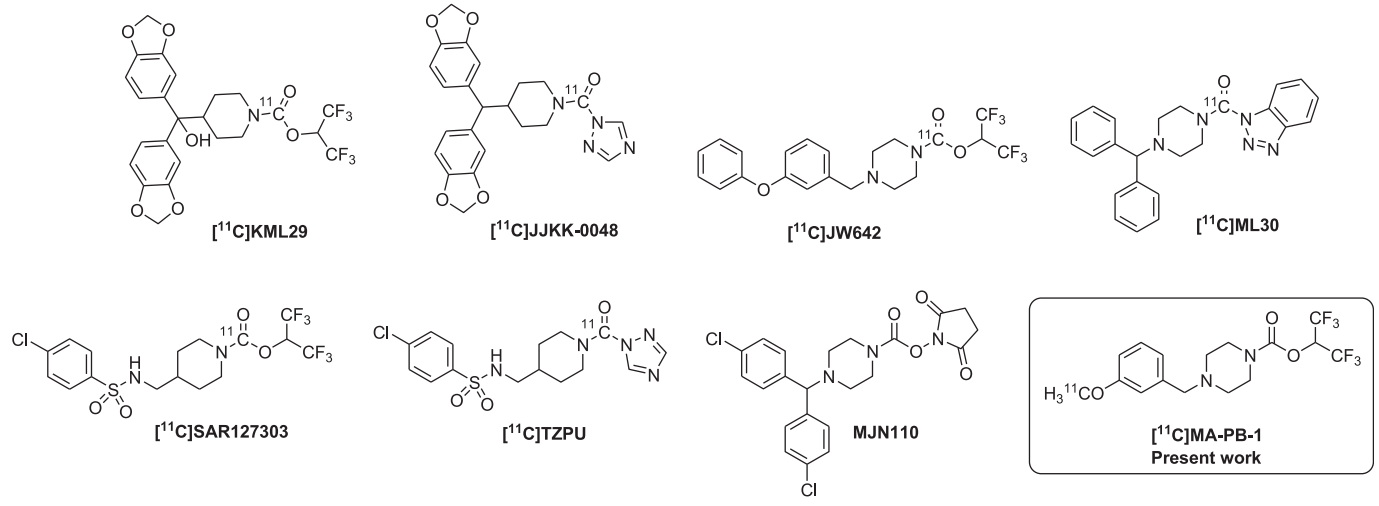

Structures of recently reported MAGL PET tracers and of MA-PB-1 (radiotracer developed and studied in this work), MJN 110 MAGL inhibitor used for blocking studies.

Hicks and co-workers reported PET radioligands for imaging of MAGL [26]. Four ligands labeled with carbon-11 at a carbonyl carbon, namely [^{11}C]-KML29, [^{11}C]-JW642, [^{11}C]-ML-30 and [^{11}C]-JJKK-0048 and a [^{11}C]CH_3-labeled 1,2,4-triazole urea compound were studied. These compounds were reported to have moderate BBB penetration (0.2–0.8 SUV at 2 and 40 min in mice), but brain retention could not be self-blocked. The lack of MAGL-specific brain uptake led to the conclusion that none of the tracers was suitable for *in vivo* imaging of brain MAGL. While preparing this manuscript, Hooker et al. published [^{11}C]-SAR127303 as a specific MAGL tracer in rats [23] and Liang et al. published comparative study between [^{11}C]-SAR127303 and [^{11}C]-TZPU [24]. In their results [^{11}C]-TZPU does not show adequate brain penetration whereas [^{11}C]-SAR127303 does display good brain penetration and awaits further evaluation in non-human primates.

In this study, we modified the structure of JW642 in which the phenoxy group is substituted with a methoxy group resulting in MA-PB-1. We herein report the synthesis, radiosynthesis and preliminary biological evaluation of [^{11}C]MA-PB-1 for *in vivo* imaging of MAGL with PET.

2. Results and discussion

Non-invasive imaging of MAGL using PET will allow quantification of regional enzyme expression *in vivo* in healthy and pathological conditions. In general, a successful PET ligand should provide a clear specific signal (signal/noise ratio $\geq$ 1.5) to allow quantitative mapping of the target of interest. Ideally, a brain PET tracer should have a high binding affinity with $B_{max}/K_d \geq 10$ and a log D of 2–3.5 with PSA value of less than 90 Å^2 for adequate brain penetration and optimum specific to nonspecific activity ratio [30–32].

2.1. Chemistry

Synthesis of the target compounds MA-PB-1 and MA-PB-2 were carried out based on literature procedures [16] (Scheme 1). Compound **4** was synthesized by $NaBH(OAc)_3$ mediated reductive amination followed by boc deprotection using trifluoroacetic acid (TFA). After complete conversion (monitored by LC-MS) the reaction mixture was neutralized, extracted (DCM/H_2O), dried and used in the next step without any further purification. The free amine **4** was converted into MA-PB-1 by adding **4** to a mixture of hexafluoroisopropanol and triphosgene with DIPEA as a base. Finally, MA-PB-1 was demethylated with BBr_3 to yield the phenol precursor MA-PB-2.

2.2. In vitro affinity studies

Table 1 compares the *h*MAGL IC_{50} values and the clog D and cPSA values of various reported MAGL inhibitors. IC_{50} values should be interpreted with caution as values were compiled from

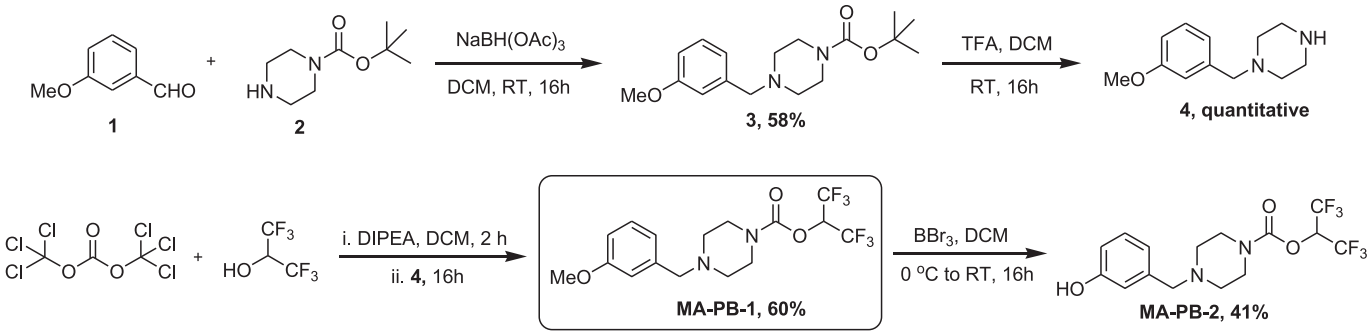

Scheme 1. Synthesis of reference and precursor.

Table 1
MAGL inhibitors along with their corresponding IC_{50} values, and calculated log D and calculated polar surface area (PSA) values (using Marvin sketch 14.11.10.0), *results from our assays.

	IC_{50} (*h*MAGL)	clog D (pH 7.4)	cPSA (Å^2)
KML29	5.9[16] (3.6[20]) nM	4.3	86.7
JJKK-048	0.4[20] nM	2.4	87.9
JW642	37.0*(3.7[16]) nM	5.0	42.0
SAR127303	29.0[23] nM	3.7 (1.9[23])	75.7
ML30	0.5[17] (1.5[20]) nM	3.9	54.3
TZPU	35.9[24] nM	0.9 (0.7[24])	97.2
MA-PB-1	26.0* nM	3.4	42.0
MJN110	11.0* (9.1[25]) nM	3.1	66.9

literature reports and were thus not obtained using the same assay except for JW642, MA-PB-1 and MJN110 which were assayed in this study.

JW642 was reported to have a *h*MAGL IC_{50} of 3.7 nM [16] and calculated log D and PSA values of 5.0 and 42.0, respectively. In our experiments assessing hMAGL-catalyzed hydrolysis of 2-AG [21,22] we observed an IC_{50} of 37 nM for JW642. In the parallel assay, we found an IC_{50} (*h*MAGL) value of 26 nM for MA-PB-1. Calculated log D and PSA values of MA-PB-1 were 3.4 and 42.0, respectively. The substitution of the phenoxy with a methoxy group although not affecting inhibitor potency in a statistically significant manner decreased the clog D value and is still within the good range for efficient BBB passage.

2.3. Radiochemistry

The radiolabeled compound [^{11}C]MA-PB-1 was obtained by alkylation of the phenolic precursor (MA-PB-2) with [^{11}C]methyl iodide at 70 °C in DMF in the presence of a base (Fig. 1).

[^{11}C]MA-PB-1 was synthesized with a radiochemical yield of 40% (n = 11, based on HPLC recovered activity). The radiolabeled reaction product could be efficiently purified from unreacted precursor and other chemical and radiochemical impurities using the described preparative HPLC system, resulting in [^{11}C]MA-PB-1 with a high radiochemical purity (≥99%) and high specific activity (58–400 GBq/μmol, n = 11), in a total synthesis time of 45 min.

2.4. Ex vivo biodistribution and regional brain distribution in mice

The data of the baseline biodistribution studies are summarized in Fig. 2 and show a transient accumulation of [^{11}C]MA-PB-1 in liver (14.4 %ID at 60 min p.i.) with transfer to the intestines (12.8 %ID at 60 min p.i.). This can be explained by the lipophilic nature of the compound resulting in hepatobiliary clearance from the blood. Apart from the hepatobiliary clearance, [^{11}C]MA-PB-1 showed a significant clearance through the renal pathway (7.9 %ID in bladder plus urine at 60 min p.i.). Despite the excretion through both the renal and hepatobiliary system, clearance of [^{11}C]MA-PB-1 from blood was rather slow (3.8 ± 0.2% ID at 60 min p.i.). This retention does not seem to be caused by MAGL binding of [^{11}C]MA-PB-1 in blood cells or plasma [33] as we did not observe any blocking effect in the blood (Fig. 3). However, plasma radiometabolite analysis indicated fast metabolism with only 6% of the intact [^{11}C]MA-PB-1 present in blood at 30 min p.i. Retention of radiometabolites in the blood may thus explain the slow blood clearance.

Importantly, [^{11}C]MA-PB-1 showed a high brain uptake (average $SUV_{whole\ brain}$ = 2.6 at 2 min p.i.) which can be explained by its favourable clog D and cPSA values (Table 1). Investigation of the regional brain distribution of the tracer showed a uniform distribution of [^{11}C]MA-PB-1 amongst the studied brain regions (Fig. 3) which are in accordance to the reported uniform MAGL distribution in the brain [34]. After the high initial uptake, [^{11}C]MA-PB-1 partially washed out followed by accumulation in the brain between 10 and 60 min to reach a steady state concentration ($SUV_{total\ brain}$ = 1.6 ± 0.3). These observations are in accordance with the kinetics of an irreversible tracer. Because of the retention of tracer in the brain, high brain-to-blood ratios (calculated as SUV brain/SUV blood) were achieved (4.1 and 3.7 at 30 and 60 min p.i., respectively) despite the slow clearance of radioactivity from the blood.

In order to verify the binding specificity, biodistribution studies were performed at 30 and 60 min post tracer injection in mice that were pretreated with cold MA-PB-1 (10 mg/kg, i.p.) 60 min before injection of the tracer. Additionally, a blocking experiment was conducted in which the biodistribution was studied at 30 min post tracer injection in mice that were injected with the non-structurally related MAGL inhibitor MJN110 (10 mg/kg, i.p.) 30 min before tracer injection. Results of both blocking experiments are shown in Fig. 3. The pretreated mice showed a significantly lower [^{11}C]MA-PB-1 retention in the brain compared to untreated animals (p = 0.0007). Whole brain SUV values were about 70% lower in mice pretreated with cold MA-PB-1 compared to vehicle-treated animals at both the 30 and 60 min post tracer injection sacrification time points. As a result, brain-to-blood ratios were significantly lower in the MA-PB-1 pretreated mice (1.2 and 1.1 at 30 and 60 min p.i., respectively). Pretreatment of animals with MJN110 also resulted in a significant reduction of total [^{11}C]MA-PB-1 retention (SUV = 0.7 ± 0.1, 30 min p.i.) in the brain compared to vehicle treated animals. It is noteworthy that blocking studies performed at 1 mg/kg, 5 mg/kg and 10 mg/kg MJN110 demonstrated a significant difference in brain SUV with respect to the control. Although blocking generally follows a dose-dependent

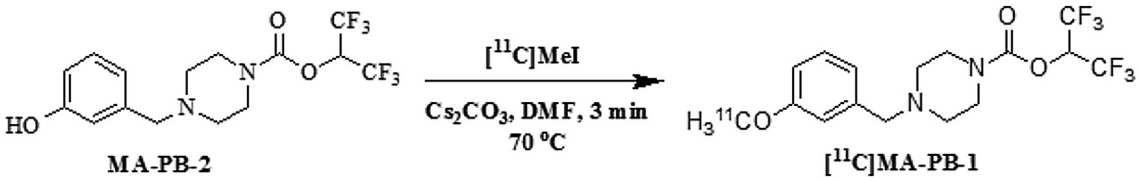

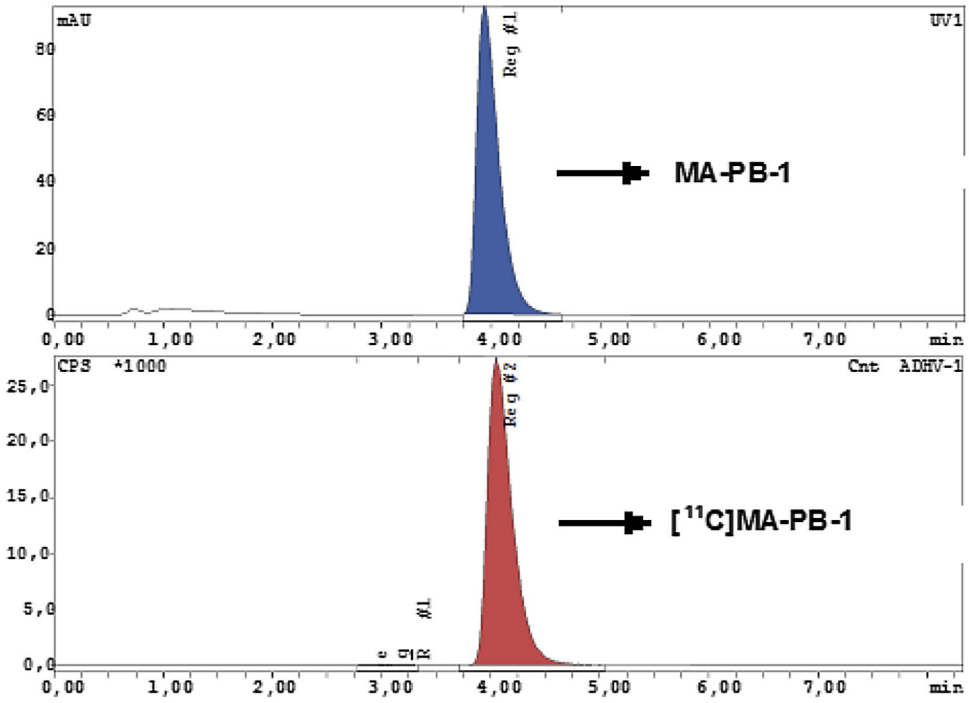

Fig. 1. MA-PB-2 was methylated with [^{11}C]MeI yielding [^{11}C]-MA-PB-1 with ≥99% radiochemical purity after preparative HPLC purification. Retention times of reference and radiolabeled MA-PB-1 were identical (co-injection of 10 μg/mL MA-PB-1 onto analytical HPLC system). Chromatographic conditions of the quality control: XBridge C18 RP column (3.5 μm, 3.0 mm × 100 mm), Mobile phase: CH_3CN/NaOAc 0.05 M pH 5.5 (55:45 v/v), Flow rate: 0.8 mL/min, detection: UV 210 nm (upper chromatogram) and radioactivity (lower chromatogram).

trend, the observed difference was not significant except between 1 mg/kg and 10 mg/kg (Fig. 4). We expected that at 1 mg/kg we would observe maximum blocking in line with previously reported results [25] but we observed stronger blocking effect after pre-treatment with 10 mg/kg. Likewise, the blocking effect was also observed in peripheral organs such as spleen, pancreas, heart and lungs, major organs where MAGL expression has been reported in various organs [34].

2.5. Plasma radiometabolite quantification in rats

Radio-HPLC of rat plasma (at 30 min post tracer injection) showed three peaks. From co-injection of plasma with authentic reference compound, we could identify the peak with retention time of approximately 10 min as intact [^{11}C]MA-PB-1. The major radiometabolite was a polar radiometabolite eluting around 4 min. A second apolar radiometabolite eluted around 15 min. Our data suggest that [^{11}C]MA-PB-1 is rapidly metabolized *in vivo*, since 30 min after injection of [^{11}C]MA-PB-1, only 6% of the radioactivity in plasma was assigned to intact parent tracer. 28% (n = 3) of plasma activity could not be extracted from the protein denatured fraction which may indicate covalent binding of the tracer to plasma.

2.6. Perfused brain radiometabolite quantification in rats

In order to quantify radiometabolites formed in or entering the brain, a perfused brain radiometabolite analysis in rats was performed. The extraction efficiency from brain was low (15–30%) suggesting irreversible binding of the tracer to brain MAGL which is associated to the pellet of denatured proteins that precipitate upon addition of CH_3CN to the brain homogenate. A relatively low amount of radiometabolites more polar than the intact tracer was found in brain (<10% of total brain activity; 90% of non-protein bound tracer at 30 min p.i.), indicating that the radiometabolites found in plasma at the same time point show limited brain uptake.

2.7. In vivo microPET studies in rats

In vivo brain distribution and kinetics of [^{11}C]MA-PB-1 were studied using microPET imaging in rats (n = 3). A group of female Wistar rats (n = 3) was scanned at baseline conditions. Additionally, a blocking and displacement study was set up using MJN110 to check the specificity and reversibility of the tracer binding. Since the same animals were used for baseline, blocking and chase experiments, each baseline scan was used as an internal reference for the other scans. An overview of the microPET results can be found in Fig. 5. Averaged microPET images in baseline conditions showed a high-intensity signal in the brain (Fig. 5A). Analysis of the

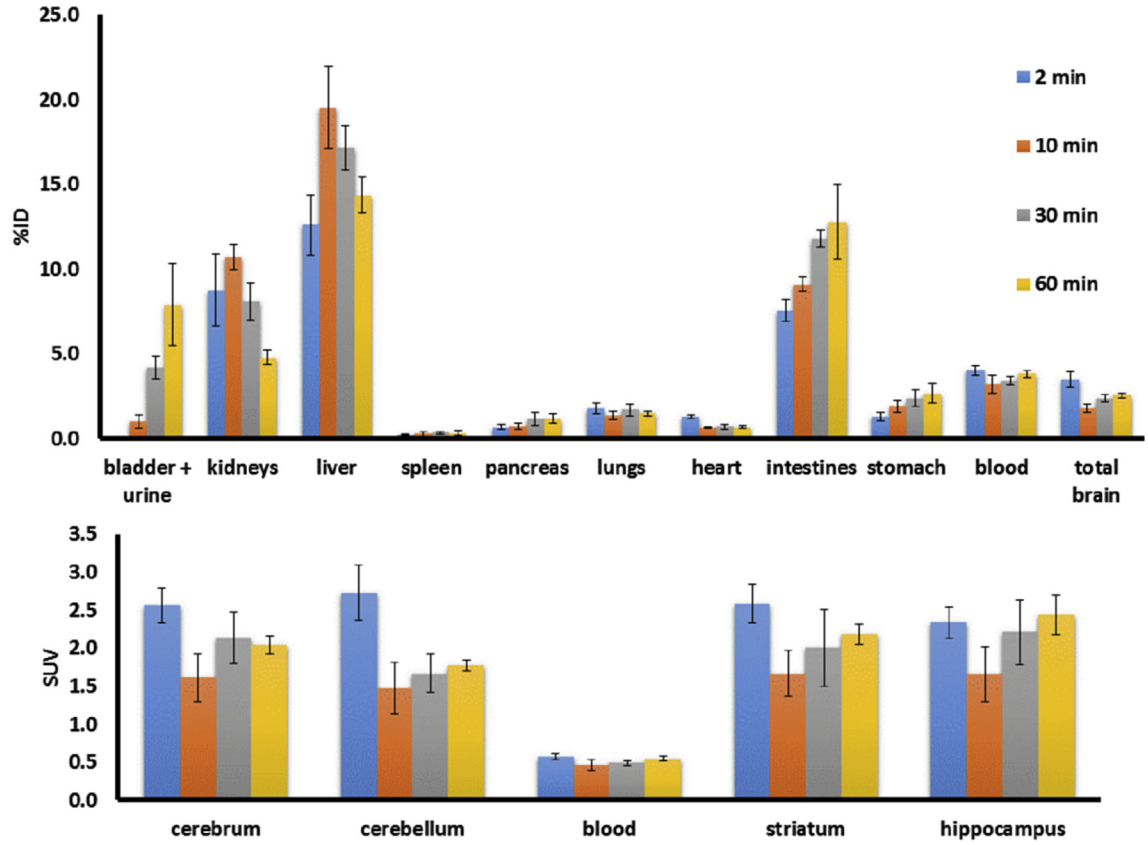

Fig. 2. Biodistribution and regional brain distribution of [^{11}C]MA-PB-1 in mice at 2, 10, 30 and 60 min post tracer injection in baseline conditions. The top figure shows the general distribution (% ID) of the tracer in adult female NMRI mice at different time points post-injection (n = 4/time point). The bottom figure shows the relative regional brain and blood concentrations (SUV) at different time points post-injection (n = 4/time point).

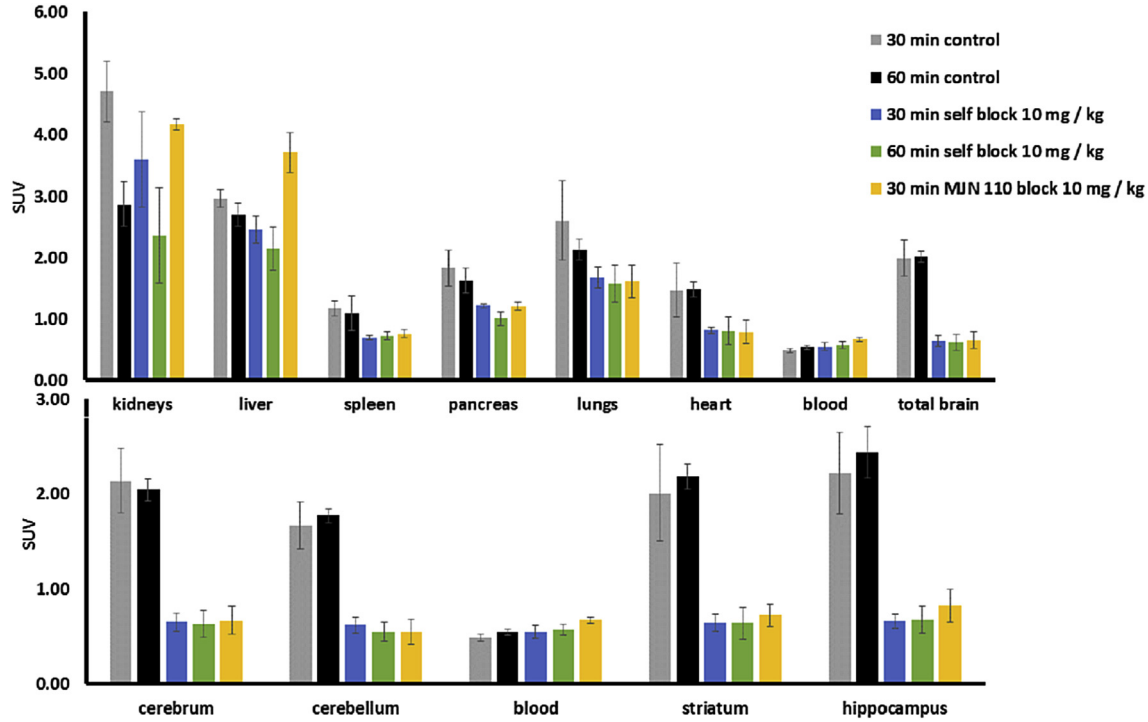

Fig. 3. Biodistribution and regional brain distribution of [^{11}C]MA-PB-1 in mice at 30 min and 60 min p.i. in baseline conditions and 30 or 60 min after pretreatment with cold MA-PB-1 (10 mg/kg i.p.) and 30 min after pretreatment with MJN110 (10 mg/kg, i.p.). The concentration in the different organs, brain regions and fluids is expressed as SUV values.

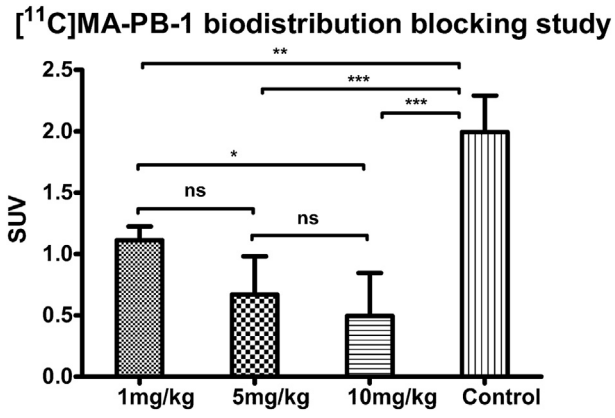

Fig. 4. Blocking study with 1 mg/kg, 5 mg/kg and 10 mg/kg doses of MJN110 compared with control conditions. (ns = $P \geq 0.05$, * = $P \leq 0.05$, ** = $P \leq 0.01$, *** = $P \leq 0.001$). Results expressed as SUV in mouse brain at 30 min post tracer injection.

corresponding time-activity curves (TACs) showed retention of [^{11}C]MA-PB-1 in the brain. After high initial uptake of [^{11}C]MA-PB-1 (SUV of ~1.6 at 2 min), activity in the brain rapidly decreased to reach stable values starting from 20 min p.i. (average SUV whole brain 30–90 min = 0.6). The initial brain uptake of [^{11}C]MA-PB-1 (1.6 and 2.6 SUV in rats and mice, respectively at 2 min p.i.) is comparable with the recently reported [^{11}C]-SAR127303 tracer [23] (SUV value of 1.7 at 2 min in rats) and 4 times higher than [^{11}C]-TZPU [24] (SUV value 0.4 at 2 min in rats). In vivo studies with [^{11}C]-SAR127303 and [^{11}C]-TZPU showed that the radioactivity in brain remained stable with no significant clearance even after 60 min. However with [^{11}C]MA-PB-1 after the high initial brain uptake, a significant washout from rat brain was observed, with SUV values decreasing from ~1.6 at 2 min p.i. to ~0.6 at 60 min p.i. (Fig. 5D). This is in contrast with the biodistribution results obtained in mice, where the radioactivity in brain remained stable even at 60 min p.i. and likely this could be attributed to species difference (Fig. 2).

Specificity of [^{11}C]MA-PB-1 binding to MAGL *in vivo* was tested in a blocking study in which the same rats from the baseline scan (n = 3) were pre-treated with the structurally unrelated MJN110 (10 mg/kg, i.p., 30 min before tracer injection). After blocking, the retention of [^{11}C]MA-PB-1 in the brain was significantly reduced resulting in only background signal in the brain (Fig. 5B). The significant blocking effect could also be observed *via* the TAC analysis. Equilibrium SUV values in the different brain regions (average SUV total brain $_{30min-90min}$ = 0.26) were about 60% lower compared to SUV values in baseline conditions acquired in the same rats. Pre-treatment with cold MA-PB-1 also showed a significant blocking effect both in *ex vivo* biodistribution and *in vivo* micro-PET studies (data not shown). These microPET data confirm that a high proportion of the [^{11}C]MA-PB-1 specifically binds to brain MAGL *in vivo* in rats as was also observed in biodistribution studies in mice.

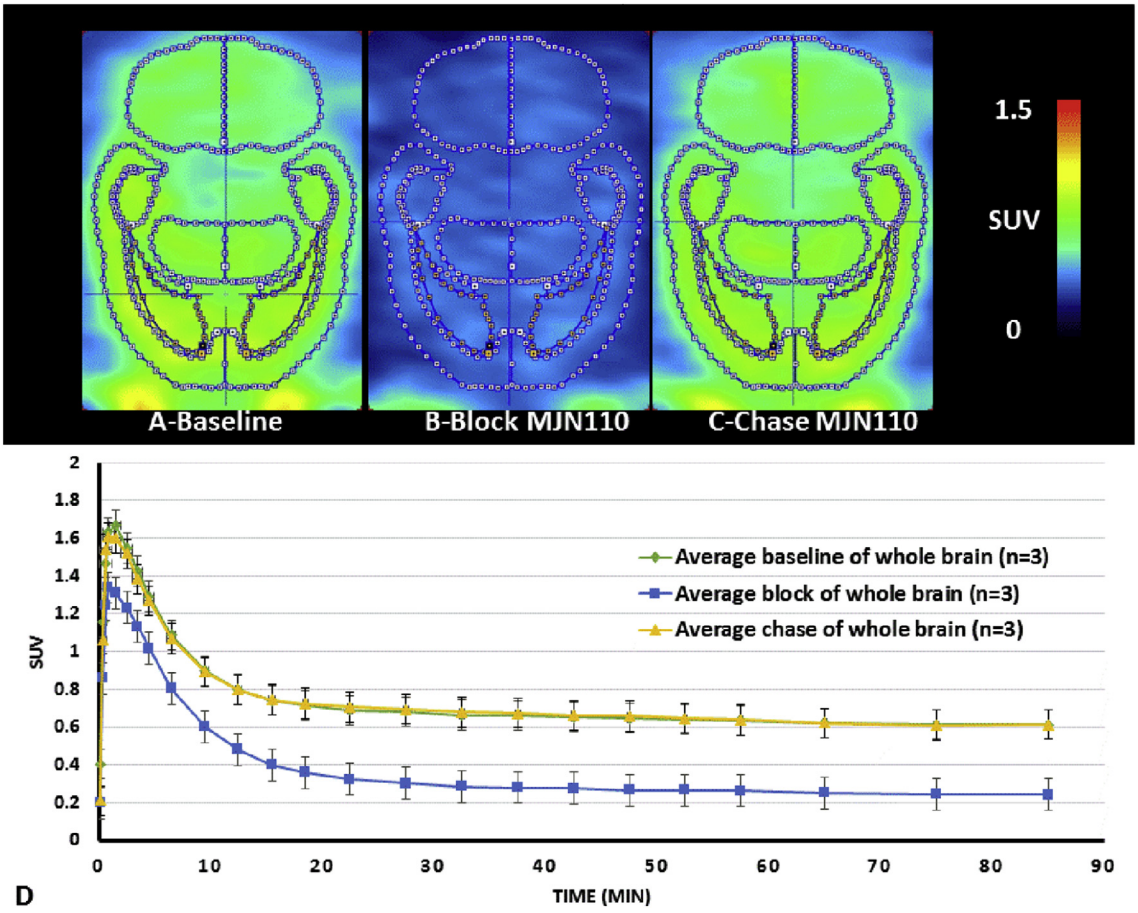

Fig. 5. MicroPET images (horizontal section) showing brain distribution and corresponding TACs describing brain kinetics after i.v. injection of 55 MBq [^{11}C]MA-PB-1 in rats under gaseous anesthesia (isoflurane 2.5% in O_2, 1 L/min). The top figure shows averaged summed images (0–90 min) from three animals: baseline (A), after blocking with MJN110 (10 mg/kg i.p. 30 min before tracer injection, B) and after a chase with MJN110 (10 mg/kg i.v. 20 min after tracer injection, C). The graph (D) shows the TACs, the average whole brain kinetics in baseline conditions, after blocking and in chase conditions as a function of time.

Finally, in a microPET displacement study, the same rats (n = 3) were injected with [^{11}C]MA-PB-1 followed by an *i.v.* challenge with MJN110 (10 mg/kg) at 20 min post tracer injection. An averaged microPET image of all three rats in the chase experiment is shown in Fig. 5C. TACs of the brain after chase are similar to those acquired in baseline conditions. This lack of displacement of radioactivity after injection of a high dose of MJN110 was expected due to the irreversible nature of the [^{11}C]MA-PB-1 binding. Similarly, Hooker et al. performed a chase study by injection of cold SAR127303 (20 min p.i. of [^{11}C]-SAR127303) and observed that brain uptake was not affected.

2.8. Non-human primate rhesus monkey microPET

The results of the 90-min baseline and pre-treatment scan of [^{11}C]MA-PB-1 in monkey are shown in Fig. 6. TACs of the baseline scan of [^{11}C]MA-PB-1 in the brain show a fast and high initial brain uptake (SUV of ~4.2 in the whole brain, time to peak uptake: 2.5 min). After 20 min the brain activity reaches a steady state (SUV value of about 2.5), suggesting irreversible binding of the radiotracer. For comparison, the brain SUV of [^{11}C]-SAR127303 gradually increased as a function of time to reach about 0.8 at steady state. A homogeneous distribution of [^{11}C]MA-PB-1 was recorded in all observed brain regions, with lower initial uptake in the caudate and highest in prefrontal cortex. The SUV signal of the pre-treatment scan was decreased (SUV of 1 after 20 min and 0.3 after 40 min in the whole brain).

3. Conclusion

We successfully synthesized MA-PB-1, and radiolabeled [^{11}C] MA-PB-1 in good yields, and high radiochemical purity and specific radioactivity. Substitution of the phenoxy group with a methoxy group in JW642 although not affecting inhibitor potency in a statistically significant manner, decreased the clog D which may contribute to increased brain exposure of MA-PB-1. Significant brain uptake of [^{11}C]MA-PB-1 was observed in biodistribution and microPET imaging experiments in mice, rats and monkey. Self-blocking experiments confirmed the specificity of binding. Blocking and chasing studies with the structurally non-related MAGL

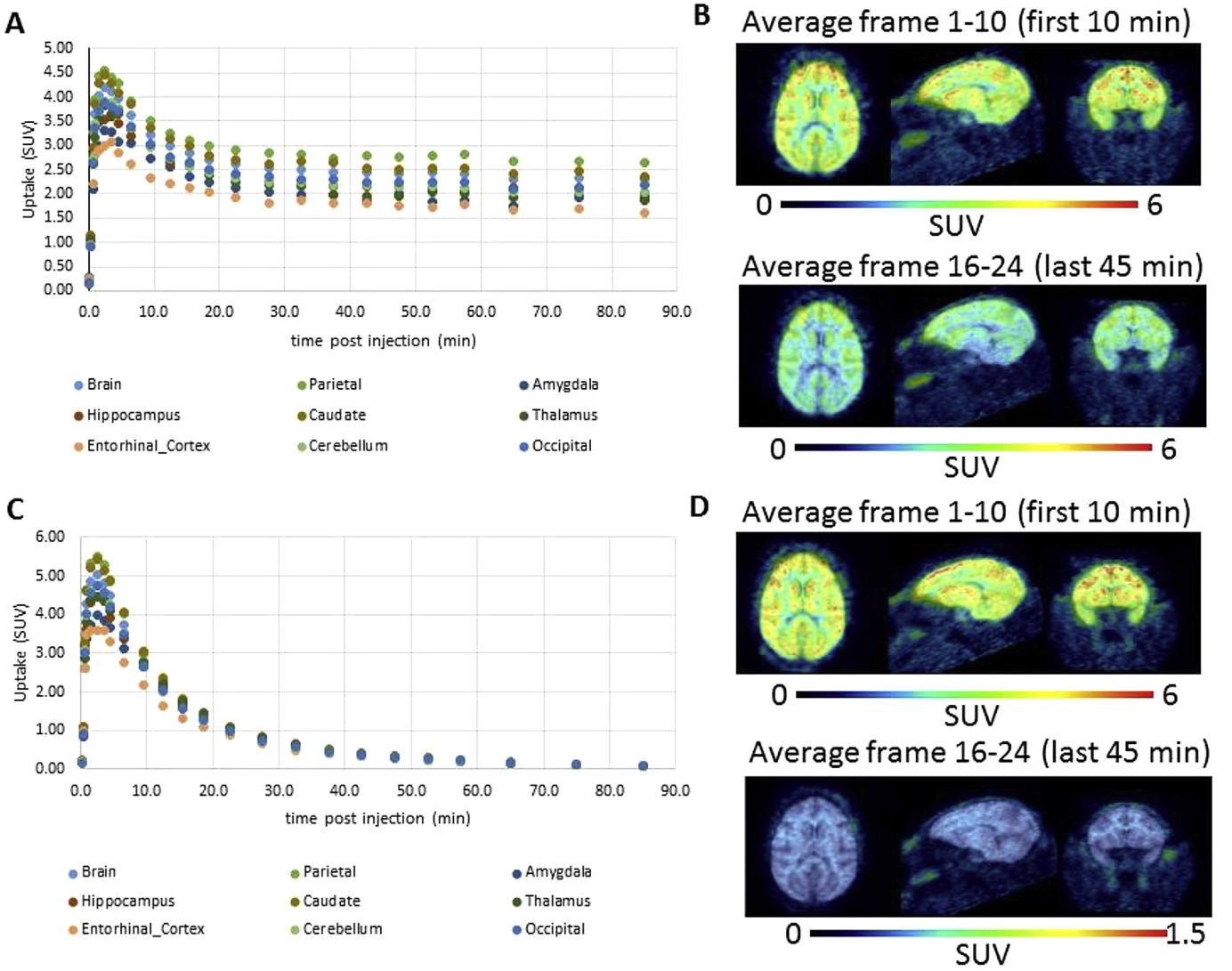

Fig. 6. μPET TACs for [^{11}C]MA-PB-1 of the whole monkey brain and of various brain regions: Baseline (A) and after pre-treatment with MJN110 (1 mg/kg i.v. 10 min before tracer injection, C). Transversal, sagittal and coronal μPET images of the baseline (B) and pre-treatment (D) experiment with [^{11}C]MA-PB-1: averaged images from 1 to 10 min and from 45 to 90 min after tracer injection.

inhibitor MJN110 in mice, rats and monkey established [^{11}C]MA-PB-1 as a MAGL specific irreversible tracer meriting further evaluation.

4. Materials and methods

4.1. General materials and methods

All the chemicals employed in the synthesis were purchased from commercially reliable suppliers (Aldrich, TCI Europe or ACROS) and used without further purification unless stated. ^{1}H and ^{13}C Nuclear magnetic resonance (NMR) spectra were obtained on a 400 MHz and 101 MHz Bruker NMR spectrometer in the deuterated solvents as indicated and with tetramethylsilane, TMS ($\delta = 0$), as an internal standard. Chemical shifts (δ) are reported in ppm and coupling constants are reported in Hertz. Multiplicity is defined by s (singlet), d (doublet), t (triplet), and m (multiplet). The mass spectra were recorded on a Bruker maXis impact UHR-TOF mass spectrometer coupled to a Dionex 3000RS UHPLC system (Bruker-Daltonik, Bremen, Germany).

High performance liquid chromatography (HPLC) was performed using a Shimadzu LC-2010A HT system connected to a UV spectrometer. Radioactivity in the column eluent was monitored using a 3-in NaI(Tl) scintillation detector connected to a single channel analyzer (Gabi box, Raytest, Straubenhardt, Germany). Radioactivity in samples of biodistribution studies and radiometabolite analysis was quantified with an automated gamma counter, equipped with a 3-in NaI(Tl) well crystal coupled to a multichannel analyzer (Wallac 1480 Wizard, Wallac, Turku, Finland). The results were corrected for background radiation, detector dead-time and physical decay during counting.

All animals were housed in individually ventilated cages in a thermoregulated (22 °C) and humidity-controlled environment under a 12 h/12 h day/night cycle with free access to food and water. All animal experiments were approved by the local Animal Ethics Committee of the University of Leuven (P104/2016) and was in accordance with European Ethics Committee guidelines (decree 86/609/EEC).

4.2. Chemistry

4.2.1. Tert-butyl 4-(3-methoxybenzyl)piperazine-1-carboxylate, **3**

To a solution of 3-methoxy benzaldehyde, **1** (1.0 g, 7.34 mmol, 1 eq) and *N*-Boc piperazine, **2** (1.05 g, 8.08 mmol, 1.1 eq) in dichloromethane (DCM, 10 mL) at 0 °C was added portionwise $NaHB(OAc)_3$ (1.87 g, 8.81 mmol, 1.2 eq) and the mixture was stirred at room temperature (RT) for 16 h. The reaction mixture was diluted with DCM (150 mL) and washed with H_2O (2 × 30 mL) and with brine (30 mL). The organic layers were dried over anhydrous $MgSO_4$ and evaporated under reduced pressure. The crude residue was purified by flash column chromatography using 0–50% EtOAc/heptane mixtures to give compound **3** as a colorless oil (1.30 g, 58%).

^{1}H NMR ($CDCl_3$, 400 MHz): δ 1.45 (s, 9H, Boc), 2.37–2.40 (m, 4H, $2CH_2$), 3.40–3.44 (m, 4H, $2CH_2$), 3.48 (s, 3H, OMe), 3.80 (s, 1H, CH_2), 6.79 (d, 1H, *J* 8.0, Ar), 6.87–6.90 (m, 2H, Ar), 7.22 (t, 1H, *J* 7.9, Ar). ^{13}C NMR ($CDCl_3$, 101 MHz): δ 28.61, 53.05, 55.38, 63.15, 79.72, 112.70, 114.78, 121.61, 129.40, 139.75, 154.98, 159.83. HRMS (ESI) Calcd. for $C_{17}H_{27}N_2O_3$ $(M+H)^+$: 307.2016. Found: 307.2071.

4.2.2. 1,1,1,3,3,3-Hexafluoropropan-2-yl 4-(3-methoxybenzyl) piperazine-1-carboxylate, ***MA-PB-1***

To a solution of triphosgene (0.185 g, 0.624 mmol, 0.33 eq) in dry DCM (5 mL) were added hexafluoroisopropanol (0.197 mL, 1.892 mmol, 1 eq) and diisopropylethyl amine (DIPEA, 0.346 mL, 3.784 mmol, 2 eq) and the reaction mixture was stirred for 2 h at RT under N_2. Compound **3** was boc deprotected using TFA in DCM, the free amine **4** (0.390 g, 1.892 mmol, 1 eq) in DCM (2 mL) was added and the reaction mixture was further stirred at RT for 3 h. The mixture was diluted with DCM (100 mL) and washed with H_2O (2 × 10 mL) and with brine (20 mL). The organic layers were dried over anhydrous $MgSO_4$ and evaporated under reduced pressure. The crude residue was purified by flash column chromatography using EtOAc/heptane mixtures to give MA-PB-1 as pale yellow oil (0.455 g, 60%).

^{1}H NMR ($CDCl_3$, 400 MHz): δ 2.42–2.47 (m, 4H, $2CH_2$), 3.50 (s, 2H, CH_2), 3.54–3.58 (m, 4H, $2CH_2$), 3.80 (s, 3H, OMe), 5.73–5.78 (m, 1H, CH), 6.80 (d, 1H, *J* 8.0, Ar), 6.78 (s, 1H, Ar), 6.89 (d, 1H, *J* 7.2, Ar), 7.23 (t, 1H, *J* 7.9, Ar). ^{13}C NMR ($CDCl_3$, 101 MHz): δ 41.12, 41.52, 49.06, 49.29, 51.93, 59.48, 64.60, 109.38, 111.34, 118.09, 126.08, 135.93, 148.15, 156.48. HRMS (ESI) Calcd. for $C_{16}H_{19}F_6N_2O_3$ $(M+H)^+$: 401.1294. Found: 401.1296. HPLC purity: >98%.

4.2.3. 1,1,1,3,3,3-Hexafluoropropan-2-yl 4-(3-hydroxybenzyl) piperazine-1-carboxylate, ***MA-PB-2***

To a solution of MA-PB-1 (100 mg, 0.25 mmol) in DCM (5 mL) at 0 °C, BBr_3 (~0.3 mL) was added and stirred. After 30 min the reaction mixture was allowed to warm to RT and stirred for about 16 h. The mixture was neutralized to pH 7, diluted with DCM (50 mL) and washed with H_2O (2 × 10 mL) and with saturated $NaHCO_3$ solution (20 mL). The organic layers were dried over anhydrous $MgSO_4$ and evaporated under reduced pressure. The crude residue was purified by flash column chromatography using EtOAc/heptane mixtures to give MA-PB-2 as a colourless powder (97 mg, 41%).

^{1}H NMR ($CDCl_3$, 400 MHz): δ 2.44–2.47 (m, 4H, $2CH_2$), 3.47 (s, 2H, CH_2), 3.52–3.56 (m, 4H, $2CH_2$), 5.70–5.75 (m, 1H, CH), 6.71 (d, 1H, *J* 8.0, Ar), 6.78 (d, 1H, Ar), 6.87–6.90 (m, 2H, Ar), 7.16 (t, 1H, *J* 7.4, Ar). ^{13}C NMR ($CDCl_3$, 101 MHz): δ 44.30, 44.68, 52.48, 52.70, 53.62, 62.82, 68.32, 114.92, 116.32, 121.69, 129.84, 138.87, 151.64, 156.18. HRMS (ESI) Calcd. for $C_{15}H_{17}F_6N_2O_3$ $(M+H^+)$: 387.1137. Found: 387.1140.

4.3. Radiosynthesis

[^{11}C]MeI was produced according to the procedure described by Andrés et al. [27]. and bubbled with a stream of helium through a solution of the radiolabeling precursor (200 μg) and Cs_2CO_3 (1–3 mg) in anhydrous DMF (200 μL). The mixture was then heated for 3 min at 70 °C. After dilution with 1 mL water, the crude reaction mixture was purified by HPLC using an XBridge C_{18} column (5 μm, 4.6 mm × 150 mm; Waters, Milford, Connecticut) eluted with a mixture of 0.05 M sodium acetate buffer pH 5.5 and EtOH (43/57 v/v) at a flow rate of 1 mL/min. UV monitoring of the eluate was performed at 254 nm. The peak corresponding to [^{11}C]MA-PB-1 was collected, diluted with saline to obtain a final ethanol concentration of <10% and sterile filtered through a 0.22-μm membrane filter (Millex GV 13 mm; Millipore, Billerica, MA). The chemical and radiochemical purity of the tracer was assessed using HPLC on an analytical XBridge C_{18} column (3.5 μm, 3.0 mm × 100 mm, Waters) eluted with a mixture of a 0.05 M sodium acetate buffer pH 5.5 and acetonitrile (45/55 v/v) at a flow rate of 0.8 mL/min. UV detection was done at 210 nm. Identity of the tracer was confirmed by co-elution with authentic cold reference on the same HPLC.

4.4. Biological evaluation

4.4.1. MAGL activity assay

A sensitive fluorescence-based hydrolase assay detecting formation of glycerol was used to determine the rate of hMAGL-

catalyzed hydrolysis of the natural monoacylglycerol substrate 2-AG as well as to determine the potency of MAGL inhibitors (IC_{50} values) in a 96-well format, essentially as previously described [21,22]. The amount of hMAGL-lysate protein per well was 0.3 μg. This methodology has been previously used allowing comparison of potencies between various MAGL inhibitors, such as JJKK-048, ML30, KML29 and IDFP, under identical experimental conditions [20].

4.4.2. Biodistribution

Biodistribution studies were carried out in healthy adult female NMRI mice (body mass 29–50 g) at 2, 10, 30 and 60 min post injection (p.i.) (n = 4 per time point). Additional biodistribution studies (30 and 60 min post tracer injection, n = 4 per time point) were performed 60 min after pretreatment with cold MA-PB-1 (10 mg/kg; subcutaneous (s.c.) administration) or 30 min after pretreatment with MJN110 (10 mg/kg; s.c. administration). MA-PB1 and MJN110 were dissolved in a vehicle containing 10% DMSO, 10% 2-hydroxypropyl β-cyclodextrin and 5% tween 80 in saline at a concentration of 2 mg/mL. During the procedure, mice were anesthetized with 2.5% isoflurane in O_2 at a flow rate of 1 L/min and injected with about 9 MBq of tracer *via* a tail vein. The animals were then sacrificed by decapitation at above specified time points post tracer injection. Blood and major organs were collected in tared tubes and weighed. The radioactivity in blood, organs and other body parts was counted using an automated gamma counter. For calculation of the total radioactivity in blood, blood mass was assumed to be 7% of the total body mass [28].

4.4.3. Plasma radiometabolite quantification in rats

Healthy Wistar rats (n = 3) were anesthetized with isoflurane (2.5% in O_2 at 1 L/min) and injected intravenously (*i.v.*) with about 55 MBq of the tracer *via* a tail vein. At 30 min p.i., the rats were sacrificed by decapitation and blood was collected in tubes containing 7.2 mg K_2EDTA (BD vacutainer, BD, Franklin Lakes, NJ) and stored on ice. The blood was centrifuged for 10 min (2330 × g) to separate plasma. To about 0.5 mL of plasma an equal amount of acetonitrile was added and the solution was vortexed and centrifuged for 5 min (2330 × g) to separate the precipitated proteins from the supernatant. Further, 0.5 mL of supernatant was taken and diluted with 0.1 mL of water. It was filtered through a syringe filter (0.22 μm nylon filter, Acrodisc 13, PALL Life Sciences) and spiked with 20 μg of authentic MA-PB-1. A volume of 0.5 mL of extract was injected onto an HPLC system consisting of an analytical XBridge column (C_{18}, 5 μM, 3 mm × 100 mm, Waters) eluted with a mixture of 0.05 M sodium acetate (pH 5.5) and CH_3CN (45:55 v/v) at a flow rate of 0.7 mL/min. The HPLC eluate was collected as 1-mL fractions after passing through a UV detector (210 nm), and radioactivity in the fractions was measured using an automated gamma counter.

4.4.4. Perfused brain radiometabolite quantification in rats

Healthy Wistar rats (n = 3) were anesthetized with isoflurane (2.5% in O_2 at 1 L/min) and *i.v.* injected with about 37 MBq of [^{11}C]MA-PB-1. At 30 min p.i., they were sacrificed by an overdose of pentobarbital (Nembutal, CEVA Santé Animale, Libourne, France; 200 mg/kg intraperitoneal) followed by cardiac perfusion with saline. Brain was isolated and homogenized/denatured in 3 mL of CH_3CN, for about 2 min. After centrifugation (1710 × g, 5 min), about 1 mL supernatant was collected, diluted with 1 mL H_2O, and filtered through a 0.22-μm filter (Millipore, Bedford, MA). About 0.5 mL of the filtrate was diluted with 0.1 mL of water and spiked with 20 μg of authentic MA-PB-1. A volume of 0.5 mL of this brain homogenate extract was injected onto an HPLC system consisting of an analytical XBridge column (C_{18}, 5 μM, 3 mm × 100 mm, Waters) eluted with a mixture of 0.05 M sodium acetate (pH 5.5) and CH_3CN (45:55 v/v) at a flow rate of 0.7 mL/min. The HPLC eluate was collected as 1-mL fractions after passing through a UV detector (210 nm), and radioactivity in the fractions was measured using an automated gamma counter.

4.4.5. In vivo microPET studies in rats

MicroPET imaging experiments were performed on a Focus™ 220 microPET scanner (Concorde Microsystems, Knoxville, TN) using female Wistar rats. During the whole procedure, animals were kept under gas anesthesia (2.5% isoflurane in O_2 at 1 L/min flow rate). The animal's head was fixed and positioned central in the field of view of the microPET scanner. Upon tracer injection, a dynamic microPET scan was started for 90 min. All scans were acquired in list mode. Acquisition data were Fourier rebinned in 24 time frames (4 × 15 s, 4 × 60 s, 5 × 180 s, 8 × 5 min, 3 × 10 min) and reconstructed using maximum a posteriori iterative reconstruction. A summed image of the reconstructed data was spatially normalized to an in-house created ^{18}F-FDG template of the rat brain in Paxinos coordinates [29] using an affine transformation. The latter was then used to normalize all time frames of the dynamic microPET data set to allow automated and bilateral volumes of interest (VOIs) analyses. Time activity curves (TACs) were generated for whole brains, using PMOD software (v 3.2, PMOD Technologies, Zürich, Switzerland).

In the blocking microPET studies, rats (n = 3) were anesthetized with 2.5% isoflurane in O_2 at 1 L/min flow rate and i.p. injected with MJN110 (10 mg/kg) 30 min prior to tracer injection. For the chase study (n = 3), MJN110 (10 mg/kg) was *i.v.* administered 20 min after tracer injection. MA-PB1 and MJN110 were dissolved in a vehicle containing 10% DMSO, 10% 2-hydroxypropyl β-cyclodextrin and 5% tween 80 in saline at a concentration of 2 mg/mL.

4.4.6. Non-human primate rhesus monkey microPET

Dynamic 90 min μPET scans with [^{11}C]MA-PB-1 were acquired with a Focus 220 μPET scanner on a female rhesus monkey (*Macaca mulatta*, 5.2 kg). Sedation was performed by i.m. injection of a combination of 0.3 mL Rompun (xylazine 2% solution) and 0.35 mL Nimatek (ketamine 100 mg/mL). About 60 min after the first injection, the monkey received an additional dose of 0.15 mL Rompun and 0.175 mL Nimatek via *i.v.* injection. During the last part of the scan, dosing was done less frequently, based on the heartbeat frequency. The O_2 and CO_2 saturation in the blood and the heartbeat were constantly monitored. Temperature was regulated via a heating pad. The breathing frequency and the eye response were checked visually. The head of the animal was placed central in the field of view of the μPET scanner. The monkey was injected with 163 MBq of [^{11}C]MA-PB-1 via the vena saphena. Scans were acquired in list mode and Fourier rebinned in 24 time frames (4 × 15 s, 4 × 60 s, 5 × 180 s, 8 × 300 s, 3 × 600 s). Data were reconstructed using a 3D maximum a posteriori (3D-MAP) iterative reconstruction. TACs of the whole brain were generated using VOIs with PMOD software and radioactivity concentration in the brain is expressed as SUV as a function of time after tracer injection. For the pre-treatment study, MJN110 was dissolved in a vehicle containing 20% DMSO and 40% (2-hydroxypropyl)-β-cyclodextrin. Pre-treatment was done by *i.v.* injection of MJN110 at a dose of 1 mg/kg 10 min before tracer injection. μPET images were compared to the baseline scan, acquired in the vehicle treated monkey. Blood samples were collected during both baseline and pre-treatment scans at 10, 30 and 60 min p.i. *via* the other vena saphena and plasma was analysed for radiometabolites according to the same procedure as described for rats (see above).

4.5. Data and statistical analysis

Quantitative data expressed as mean ± SD. Means were compared using an unpaired two-tailed student t-test. Values were considered statistically significant for $P \leq 0.05$.

Funding

This work was supported by IMIR (In Vivo Molecular Imaging Research group) at KU Leuven, Belgium also funded by the European Union's Seventh Framework Programme (FP7/2007-2013) under grant agreement no. HEALTH-F2-2011-278850 (INMiND)

Acknowledgements

We thank Dr. Jacqueline Blankman (Abide Therapeutics, USA) for the useful discussions. We also thank Julie Cornelis (Laboratory for Radiopharmacy; KU Leuven) and Ann Van Santvoort (Department of Nuclear Medicine; KU leuven) for their help with the mice and rat animal studies, Professor Wim Vanduffel and Christophe Ulens form the Laboratory of Neuro-and Psychophysiology for providing the Macaque monkey and assisting in the monkey studies.

Appendix A. Supplementary data

Supplementary data related to this article can be found at http://dx.doi.org/10.1016/j.ejmech.2017.04.066.

References

[1] L.A. Matsuda, S.J. Lolait, M.J. Brownstein, A.C. Young, T.I. Bonner, Structure of a cannabinoid receptor and function expression of the cloned cDNA, Nature 346 (1990) 561–564.
[2] N. Aaltonen, C.S. Ribas, M. Lehtonen, J.R. Savinainen, J.T. Laitinen, Brain regional cannabinoid CB1 receptor signalling and alternative enzymatic pathways for 2-arachidonoylglycerol generation in brain sections of diacylglycerol lipase deficient mice, Eur. J. Pharm. Sci. 51 (2014) 87–95.
[3] V. Di Marzo, D. Melck, T. Bisogno, L. De Petrocellis, Endocannabinoids: endogenous cannabinoid receptor ligands with neuromodulatory action, Trends Neurosci. 21 (1999) 521–528.
[4] P. Pacher, S. Batkai, G. Kunos, The endocannabinoid system as an emerging target of pharmacotherapy, Pharmacol. Rev. 58 (2006) 389–462.
[5] B.F. Cravatt, A.H. Lichtman, The endogenous cannabinoid system and its role in nociceptive behavior, J. Neurobio 61 (2004) 149–160.
[6] K. Ahn, M.K. McKinney, B.F. Cravatt, Enzymatic pathways that regulate endocannabinoid signaling in the nervous system, Chem. Rev. 108 (2008) 1687–1707.
[7] J.R. Savinainen, S.M. Saario, J.T. Laitinen, The serine hydrolases MAGL, ABHD6 and ABHD12 as guardians of 2-arachidonoylglycerol signaling through cannabinoid receptors, Acta Physiol. (Oxf.) 204 (2012) 267–276.
[8] J.L. Blankman, G.M. Simon, B.F. Cravatt, A comprehensive profile of brain enzymes that hydrolyze the endocannabinoid 2-arachidonoylglycerol, Chem. Biol. 14 (2007) 1347–1356.
[9] R.A. Kohnz, D.K. Nomura, Chemical approaches to therapeutically target the metabolism and signaling of the endocannabinoid 2-AG and eicosanoids, Chem. Soc. Rev. 43 (2014) 6859–6869.
[10] M.M. Mulvihill, D.K. Nomura, Therapeutic potential of monoacylglycerol lipase inhibitors, Life Sci. 92 (2013) 492–497.
[11] J.K. Makara, M. Mor, D. Fegley, S.I. Szabo, S. Kathuria, G. Astarita, A. Duranti, A. Tontini, G. Tarzia, S. Rivara, T.F. Freund, D. Piomelli, Selective inhibition of 2-AG hydrolysis enhances endocannabinoid signaling in hippocampus, Nat. Neurosci. 8 (2005) 1139–1141.
[12] D.K. Nomura, B.E. Morrison, J.L. Blankman, J.Z. Long, S.G. Kinsey, M.C.G. Marcondes, A.M. Ward, Y.K. Hahn, A.H. Lichtman, B. Conti, B.F. Cravatt, Endocannabinoid hydrolysis generates brain prostaglandins that promote neuroinflammation, Science 334 (2011) 809–813.
[13] Z. Cao, M.M. Mulvihill, P. Mukhopadhyay, H. Xu, K. Erdelyi, E. Hao, E. Holovac, G. Hasko, B.F. Cravatt, D.K. Nomura, P. Pacher, Monoacylglycerol lipase controls endocannabinoid and eicosanoid signaling and hepatic injury in mice, Gastroenterology 144 (2013) 808–817.
[14] C. Costola-de-Souza, A. Ribeiro, V. Ferraz-de-Paula, A.S. Calefi, T.P. Aloia, J.A. Gimenes-Junior, V.I. de Almeida, M.L. Pinheiro, J. Palermo-Neto, Monoacylglycerol lipase (MAGL) inhibition attenuates acute lung injury in mice, PLoS One 8 (2013) e77706.
[15] J.Z. Long, W. Li, L. Booker, J.J. Burston, S.G. Kinsey, J.E. Schlosburg, F.J. Pavon, A.M. Serrano, D.E. Selley, L.H. Parsons, A.H. Lichtman, B.F. Cravatt, Selective blockade of 2-arachidonoylglycerol hydrolysis produces cannabinoid behavioral effects, Nat. Chem. Biol. 5 (2009) 37–44.
[16] J.W. Chang, M.J. Niphakis, K.M. Lum, A.B. Cognetta III, C. Wang, M.L. Matthews, S. Niessen, M.W. Buczynski, L.H. Parsons, B.F. Cravatt, Remarkably selective inhibitors of monoacylglycerol lipase bearing a reactive group that is bioisosteric with endocannabinoid substrates, Chem. Biol. 19 (2012) 579–588.
[17] L. Morera, G. Labar, G. Ortar, D.M. Lambert, Development and characterization of endocannabinoid hydrolases FAAH and MAGL inhibitors bearing a benzotriazol-1-yl carboxamide scaffold, Bioorg. Med. Chem. 20 (2012) 6260–6275.
[18] G. Hernandez-Torres, M. Cipriano, E. Hedén, E. Björklund, A. Canales, D. Zian, A. Feliu, M. Mecha, C. Guaza, C.J. Fowler, S. Ortega-Gutierrez, M.L. Lopez-Rodriguez, A reversible and selective inhibitor of monoacylglycerol lipase ameliorates multiple Sclerosis, Angew. Chem. Int. Ed. Engl. 53 (2014) 13765–13770.
[19] J.Z. Patel, S. Ahenkorah, M. Vaara, M. Staszewski, Y. Adams, T. Laitinen, D. Navia-Paldanius, T. Parkkari, J.R. Savinainen, K. Walczynski, J.T. Laitinen, T.J. Nevalainen, Loratadine analogues as MAGL inhibitors, Bioorg Med. Chem. Lett. 25 (2015) 1436–1442.
[20] N. Aaltonen, J.R. Savinainen, C.R. Ribas, J. Ronkko, A. Kuusisto, J. Korhonen, D. Navia-Paldanius, J. Hayrinen, P. Takabe, H. Kasnanen, T. Pantsar, T. Laitinen, M. Lehtonen, S. Pasonen-Seppanen, A. Poso, T. Nevalainen, J.T. Laitinen, Piperazine and piperidine triazole ureas as Ultrapotent and highly selective inhibitors of monoacylglycerol lipase, Chem. Biol. 20 (2013) 379–590.
[21] J.R. Savinainen, E. Kansanen, T. Pantsar, D. Navia-Paldanius, T. Parkkari, M. Lehtonen, T. Laitinen, T. Nevalainen, A. Poso, A.L. Levonen, J.T. Laitinen, Robust hydrolysis of prostaglandin glycerol esters by human monoacylglycerol lipase (MAGL), Mol. Pharmacol. 86 (2014) 522–535.
[22] D. Navia-Paldanius, J.R. Savinainen, J.T. Laitinen, Biochemical and pharmacological characterization of human α/β hydrolase domain containing 6 (ABHD6) and 12 (ABHD12), J. Lipid Res. 53 (2012) 2413–2424.
[23] C. Wang, M.S. Placzek, G.C. Van de Bittner, F.A. Schroeder, J.M. Hooker, A novel radiotracer for imaging Monoacylglycerol lipase in the brain using positron emission tomography, ACS Chem. Neurosci. 7 (2016) 484–489.
[24] L. Wang, W. Mori, R. Cheng, J. Yui, A. Hatori, L. Ma, Y. Zhang, B.H. Rotstein, M. Fujinaga, Y. Shimoda, T. Yamasaki, L. Xie, Y. Nagai, T. Minamimoto, M. Higuchi, N. Vasdev, M.R. Zhang, S.H. Liang, Synthesis and preclinical evaluation of Sulfonamido-based [^{11}C-Carbonyl]-Carbamates and ureas for imaging monoacylglycerol lipase, Theranostics 6 (8) (2016) 1145–1159.
[25] M.J. Niphakis, A.B. Cognetta, J.W. Chang, M.W. Buczynski, L.H. Parsons, F. Byrne, J.J. Burston, V. Chapman, B.F. Cravatt, Evaluation of NHS carbamates as a potent and selective class of endocannabinoid hydrolase inhibitors, ACS Chem. Neurosci. 4 (2013) 1322–1332.
[26] J.W. Hicks, J. Parkesa, J. Tonga, S. Houlea, N. Vasdev, A.A. Wilson, Radiosynthesis and *ex vivo* evaluation of [^{11}C-*carbonyl*]carbamate- and urea-based monoacylglycerol lipase inhibitors, Nucl. Med. Biol. 41 (2014) 688–694.
[27] J.I. Andrés, M. De Angelis, J. Alcázar, L. Iturrino, X. Langlois, S. Dedeurwaerdere, I. Lenaerts, G. Vanhoff, S. Celen, G. Bormans, Synthesis, in vivo occupancy, and radiolabeling of potent Phosphodiesterase subtype-10 inhibitors as candidates for positron emission tomography imaging, J. Med. Chem. 54 (2011) 5820–5835.
[28] A.R. Fritzberg, W.P. Whitney, C.C. Kuni, W. Klingensmith, Biodistribution and renal excretion of 99mTc-N, N'-bis-(Mercaptoacetamido) ethylenediamine. Effect of renal tubular transport inhibitors, Int. J. Nucl. Med. Biol. 9 (1982) 79–82.
[29] C. Casteels, P. Vermaelen, J. Nuyts, A. Van Der Linden, V. Baekelandt, L. Mortelmans, G. Bormans, K. Van Laere, Construction and evaluation of multitracer small-animal PET probabilistic atlases for voxel-based functional mapping of the rat brain, J. Nucl. Med. 47 (2006) 1858–1866.
[30] W.C. Eckelman, R.E. Gibson, W.J. Rzeszotarski, F. Vieras, J.K. Mazaitis, B. Francis, B.,W.C. Reba, The design of receptor binding radiotracers, in: L. Colombetti (Ed.), Principles of Radiopharmacology vol. 1, CRC Press, New York, 1979, pp. 251–274.
[31] R.N. Waterhouse, Determination of lipophilicity and its use as a predictor of blood-brain barrier penetration of molecular imaging agents, Mol. Imaging Biol. 5 (2003) 376–389.
[32] V.W. Pike, PET Radiotracers: crossing the blood-brain barrier and surviving metabolism, Trends Pharmacol. Sci. 30 (2009) 431–440.
[33] C.J. Fielding, Monoglyceride hydrolase activities of rat plasma and platelets, J. Biol. Chem. 256 (1981) 876–881.
[34] M. Karlsson, J.A. Contreras, U. Hellman, H. Tornqvist, C. Holm, cDNA cloning, tissue distribution, and identification of the catalytic triad of monoglyceride lipase, J. Biol. Chem. 272 (1997) 27218–27223.